Managing light polarization via plasmon–molecule interactions within an asymmetric metal nanoparticle trimer

Timur Shegai*[†], Zhipeng Li[†‡], Tali Dadosh[§], Zhenyu Zhang[¶‖], Hongxing Xu[‡**††], and Gilad Haran*[††]

*Department of Chemical Physics, Weizmann Institute of Science, Rehovot 76100, Israel; [‡]Beijing National Laboratory for Condensed Matter Physics, Institute of Physics, Chinese Academy of Sciences, Beijing 100080, China; [§]Department of Condensed Matter Physics, Weizmann Institute of Science, Rehovot 76100, Israel; [¶]Materials Science and Technology Division, Oak Ridge National Laboratory, Oak Ridge, TN 37831; [‖]Department of Physics and Astronomy, University of Tennessee, Knoxville, TN 37996-1200; and **Division of Solid State Physics, Lund University, Box 118, S-22100 Lund, Sweden

Communicated by E. Ward Plummer, The University of Tennessee, Knoxville, TN, August 26, 2008 (received for review May 10, 2008)

The interaction of light with metal nanoparticles leads to novel phenomena mediated by surface plasmon excitations. In this article we use single molecules to characterize the interaction of surface plasmons with light, and show that such interaction can strongly modulate the polarization of the emitted light. The simplest nanostructures that enable such polarization modulation are asymmetric silver nanocrystal trimers, where individual Raman scattering molecules are located in the gap between two of the nanoparticles. The third particle breaks the dipolar symmetry of the two-particle junction, generating a wavelength-dependent polarization pattern. Indeed, the scattered light becomes elliptically polarized and its intensity pattern is rotated in the presence of the third particle. We use a combination of spectroscopic observations on single molecules, scanning electron microscope imaging, and generalized Mie theory calculations to provide a full picture of the effect of particles on the polarization of the emitted light. Furthermore, our theoretical analysis allows us to show that the observed phenomenon is very sensitive to the size of the trimer particles and their relative position, suggesting future means for precise control of light polarization on the nanoscale.

generalized Mie theory | single-molecule Raman scattering | plasmonics

Manipulating light on the nanometer scale is a challenging topic not only from a fundamental point of view, but also for applications aiming at the design of miniature optical devices. Nanoplasmonics is a rapidly emerging branch of photonics that offers variable means to manipulate light by using surface plasmon excitations on metal nanostructures (1, 2). Recent studies in the plasmonics field have mainly focused on the control of direction, intensity, and spectrum of light on the nanoscale: propagation direction and intensity. The control of the direction of light propagation was achieved by means of surface plasmon propagation in metal nanostructures (3, 4), enhanced transmission through nanoholes in optically thin metal films (5), and light beaming with a subwavelength hole (6) or hole arrays (7). The control of the intensity and spectrum of light mainly involves enhancement of the local electromagnetic field (8) by localized surface plasmon resonance (9) and plasmon coupling (10–13). A recent report about plasmon-assisted fluorescence resonance energy transfer may involve the control of both propagation and intensity of light (14), and a recent article by Ringler *et al.* (15) shows that the spectral shape of emission of fluorescent molecules can be modulated by varying the distance between particles in dimer resonators.

A less explored, yet particularly important property of light to control is its polarization. Recent work explored the sensitivity of the response of metal nanostructures to the polarization of incident light (16–18), and anisotropic L-shaped nanostructures were shown to possess some degree of birefringence (19). While our article was under review, we also became aware of an article by Taminiau *et al.* (20), in which a nano-antenna at the end of a scanning tip was used to flip the fluorescence polarization of single molecules between two directions, in-plane or out-of-plane.

Here, we employ Raman-scattered light from individual molecules to probe the response of asymmetric nanoparticle aggregates over a range of wavelengths, and to show that these aggregates can dramatically modulate the polarization of the emitted light. The simplest nanostructure for such modulation of the polarization of light is a silver nanocrystal trimer, with a single-molecule Raman scatterer located in the gap between two of the nanoparticles and the third particle acting as a wavelength-dependent polarization rotator. In the current work we provide unambiguous experimental evidence for a significant influence over the polarization of light achieved via such an asymmetric nanoparticle trimer. Theoretical simulations with the generalized Mie theory (GMT) (21, 22) show that the degree of rotation depends sensitively on the size of this particle and its distance from the first two.

Results

The response of a nanoparticle aggregate can be probed through the process of Raman scattering (RS) from a molecule residing within the aggregate. We used an inverted microscope to excite and collect RS light from nanocrystal aggregates that formed spontaneously in solution in the presence of trace concentrations of rhodamine 6G molecules (which serve as the Raman scatterers), and were deposited on a slide meshed by gold grids. The low concentration of molecules used ensured that each aggregate contained no more than a single molecule (23). A half-wave plate situated under the microscope objective was used to systematically rotate the plane of polarization of the exciting 532-nm laser and rotate back the RS light, which was then split by a polarizer into two polarized spectra, designated $I_{\parallel}(\omega)$ and $I_{\perp}(\omega)$, simultaneously recorded on a CCD camera. The half-wave plate effectively rotated the sample with respect to both the incident beam polarization and the polarizer. The gold grids on the slide were used to identify the specific aggregates from which spectra were collected in scanning electron microscope (SEM) images and obtain their geometry. Before presenting the results of these experiments we first discuss the properties of the plasmon enhancement tensors involved in the RS process.

Author contributions: T.S., Z.L., H.X., and G.H. designed research; T.S. and Z.L. performed research; T.D. contributed new reagents/analytic tools; T.S., Z.L., H.X., and G.H. analyzed data; and T.S., Z.L., Z.Z., H.X., and G.H. wrote the paper.

The authors declare no conflict of interest.

[†]These authors contributed equally to this work.

[††]To whom correspondence may be addressed. E-mail: hongxingxu@aphy.iphy.ac.cn or gilad.haran@weizmann.ac.il.

This article contains supporting information online at www.pnas.org/cgi/content/full/0808365105/DCSupplemental.

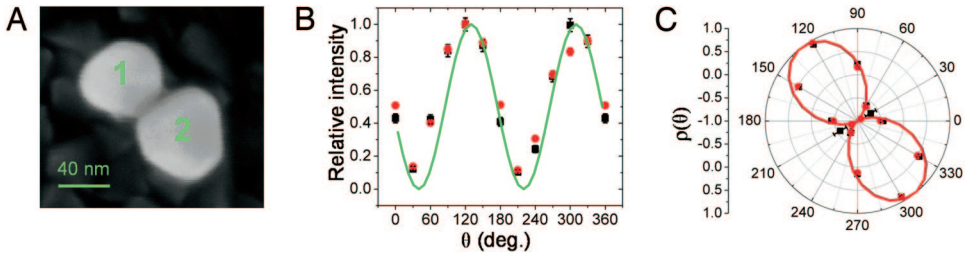

Fig. 1. Polarization response of a nanoparticle dimer. (*A*) A SEM image shows a dimer of nanoparticles, which is tilted ≈40° from the vertical direction. (*B*) Normalized RS intensity at 555 nm (black squares) and 583 nm (red circles) as a function of the angle of rotation of the incident polarization. It is seen that the maximal intensity is achieved when the incident field is polarized along the dimer symmetry axis. The green line is the result of a GMT calculation of the normalized local field enhancement factor at $\lambda = 532$ nm, by using the geometry with the radii $R_1 = 32$ nm and $R_2 = 35$ nm from the SEM image as the only input. The interparticle distance is kept at 1 nm in the junction where the molecule is assumed to locate, same as in the following figures. (*C*) Depolarization ratio (ρ) measured at 555 nm (black squares) and 583 nm (red circles). No wavelength dependence is observed and, as in the case of the intensity, the maximal depolarization ratio is achieved when the incident field is polarized along the dimer axis. Black and red lines show the results of Mie theory calculations performed at 555 and 583 nm, respectively.

The Plasmon Enhancement Tensors. Consider a molecule residing in one of the junctions formed between pairs of nanoparticles in an aggregate. The components of the electromagnetic field generated by the molecule–aggregate complex can be written as follows:

$$E = \begin{pmatrix} E_{\parallel} \\ E_{\perp} \end{pmatrix} \propto U_z^{-1}(\theta) g'(\omega_0 - \omega_{vib}) \alpha_{vib} g(\omega_0) U_z(\theta) E_0. \qquad [1]$$

Here, E_0 is the incident field. g and g' are complex-valued tensors describing the enhancement of laser field at frequency ω_0 and the enhancement of the RS field at frequency $\omega_0 - \omega_{\mathrm{vib}}$, where ω_{vib} is the frequency of a particular molecular vibrational mode. α_{vib} is the molecular polarizability tensor of this mode. U_z is a z-axis rotation operator describing the effect of the half-wave plate.

Our numerical simulations (see supporting information (SI) Fig. S1) show that the direction of the enhanced local field in the junction is always along the axis of the junction (defined as the y axis), irrespective of the incident field polarization. Similarly, the light emitted by the molecular dipole oscillating in the junction is maximally enhanced when the dipole is oriented parallel to the same axis (see Fig. S2). Therefore, the plasmon enhancement tensors can be written in the most general way as follows:

$$g(\omega_0) = \begin{pmatrix} 0 & 0 \\ g_{yx} e^{-i\phi_x} & g_{yy} e^{-i\phi_y} \end{pmatrix} \qquad [2]$$

$$g'(\omega_0 - \omega_{vib}) = \begin{pmatrix} 0 & g_{xy}' e^{i\phi_x'} \\ 0 & g_{yy}' e^{i\phi_y'} \end{pmatrix} \qquad [3]$$

where $g_{yx}, g_{yy}, g'_{xy}, g'_{yy}$ are the real values of the tensor elements and $\phi_x, \phi_y, \phi'_x, \phi'_y$ are their phases. The two tensors are related to each other by optical reciprocity, as discussed in the *SI Text*. From Eqs. **1**, **2**, and **3**, we can calculate the total (relative) intensity of emitted light and its depolarization ratio as a function of the rotation angle of the half-wave plate:

$$I = I_{\parallel} + I_{\perp} \propto \frac{1}{2}\left[1 + \frac{(r^2 - 1)\cos 2\theta + 2r\cos\Delta \sin 2\theta}{r^2 + 1}\right] \qquad [4]$$

$$\rho = \frac{I_{\parallel} - I_{\perp}}{I_{\parallel} + I_{\perp}} = \frac{(r'^2 - 1)\cos 2\theta + 2r'\cos\Delta' \sin 2\theta}{r'^2 + 1} \qquad [5]$$

In these equations $\Delta = |\phi_x - \phi_y|$ and $\Delta' = |\phi'_x - \phi'_y|$ are phase differences, whereas $r = g_{yx}/g_{yy}$ and $r' = g'_{xy}/g'_{yy}$ are ratios between tensor components. Interestingly, the intensity depends only on enhancement tensor g, whereas the depolarization ratio depends only on the emission tensor g'. Note, that such a separation can be obtained only when just one junction in a trimer is populated with molecules (this condition is trivially fulfilled in the case of single-molecule observation). If molecules reside in more than one junction, then the averaging over several geometries will not enable the separation inherent in Eqs. **4** and **5** to be obtained. In addition, the molecular polarizability tensor does not enter any of these quantities, and therefore does not affect any of the experimental observables.[‡‡] A similar conclusion was reached by Etchegoin *et al.* (24).

The Dimer Case. We consider first the simplest case of plasmon enhancement in an interparticle junction, the case of a nanocrystal dimer (11, 25). Fig. 1*A* shows the SEM image of such a dimer, and it is seen that the rotation angle of the dimer axis is ≈40° with respect to normal. Fig. 1 *B* and *C* shows (in black and red) the profiles of RS intensity and depolarization ratio for two wavelengths (555 nm and 583 nm) corresponding to two Raman bands of the molecule (773 cm^{-1} and 1650 cm^{-1}, respectively). The patterns measured at the two wavelengths coincide with each other, and their symmetry axes are along the dimer axis. Based on the geometry of Fig. 1*A* as the only input (i.e., without any free parameters), a GMT calculation, in which the two nanocrystals are represented as spheres, leads to the green curve in Fig. 1*B*, as well as the black and red curves in Fig. 1*C*. The full agreement of the calculation with the experimental result is not surprising, because, taking into account the dipolar symmetry of the dimer, it is readily shown from Eqs. **4** and **5** that the two observables take the simple forms $I \propto \sin^2\theta$ and $\rho = -\cos 2\theta$. This result, which is in agreement with previous work (18, 19, 25, 26), is of course an outcome of the axial symmetry of the dimer which thus leads to the following features: (*i*) The total intensity of the scattered light is maximized along the direction of a dimer and minimized (totally vanishes) in the direction perpendicular to it. (*ii*) The depolarization ratio is wavelength independent and reaches its maximum values of ± 1 at directions parallel (+1) and perpendicular (−1) to the dimer axis, indicating that the scattered light is linearly polarized. None of these features persist in the case of the symmetry-broken trimer, as will be shown next.

The Trimer Case. Measurements from the nanoparticle trimer shown in Fig. 2*A* are presented in Fig. 2 *B* and *C*. The RS light from a single molecule is only enhanced strongly enough for observation when the molecule is placed in a junction between two particles. Hence there are three possible locations for a

[‡‡] In a previous article (26) we suggested erroneously that single-molecule polarized surface enhanced Raman scattering (SERS) experiments can teach us about wavelength dependence of the molecular polarizability tensor.

PHYSICS

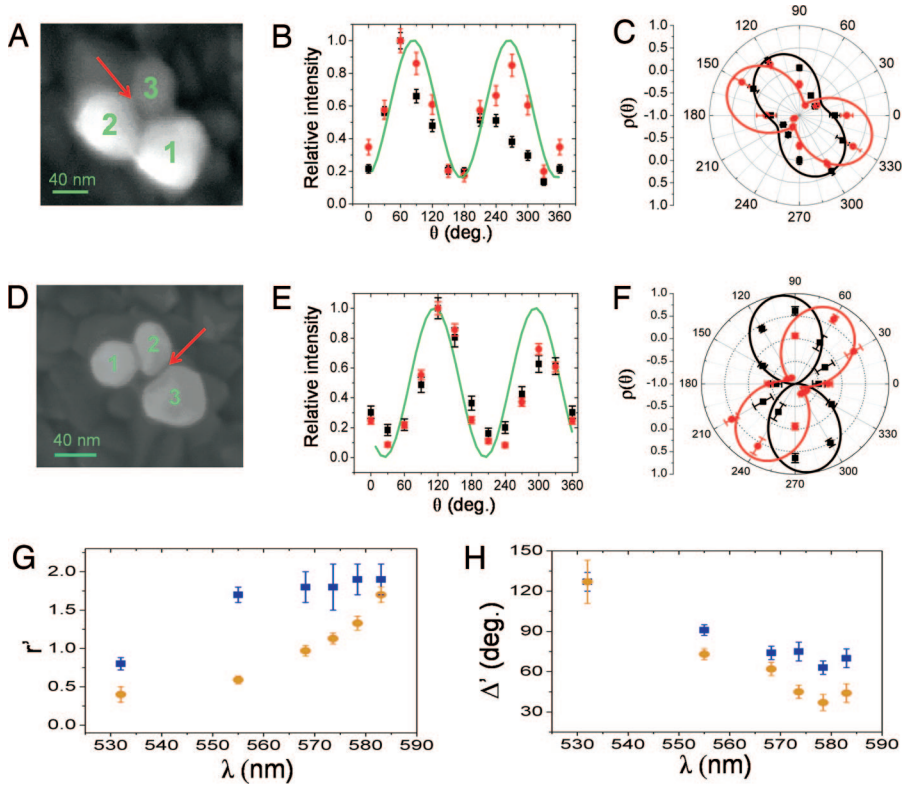

Fig. 2. Polarization response of a nanoparticle trimer. (*A*) SEM image of a trimer. A red arrow indicates the position of the molecule that leads to the best agreement between experiment and calculation. (*B*) Normalized RS intensity at 555 nm (black squares) and 583 nm (red circles) as a function of the angle of rotation of the incident polarization. The intensities at both wavelengths show approximately the same profile, but the maximal intensity is observed at ≈75°, which does not match any pair of nanoparticles in the trimer. The green line is the result of a calculation assuming that the molecule is situated at the junction with a gap of 1 nm marked with red arrow in the SEM image, and the corresponding geometrical parameters from the SEM image $R_1 = 44$ nm, $R_2 = 35$ nm, and $R_3 = 28$ nm as the input. (*C*) Depolarization ratio (ρ) measured at 555 nm (black squares) and 583 nm (red circles). Depolarization profiles are wavelength-dependent in this case, and are aligned differently than the intensity profiles. The black and red lines show the result of calculations at the two wavelengths, assuming that the molecule is situated at the junction marked with the red arrow in SEM image. (*D*) SEM image of a second trimer. A red arrow indicates the position of the molecule that leads to the best agreement between experiment and calculation. (*E*) Normalized RS intensity at 555 nm (black squares) and 583 nm (red circles) as a function of the angle of rotation of the incident polarization. As in *B*, the intensity profile does not peak along the direction of the axis connecting particles 2 and 3. (*F*) Depolarization ratio (ρ) measured at 555 nm (black squares) and 583 nm (red circles). As in *C*, depolarization profiles are wavelength-dependent, and are aligned differently than the intensity profiles. The black and red lines show the result of calculations at the two wavelengths, assuming that the molecule is situated at the junction marked with red arrow in the SEM image. (*G*) Wavelength dependence of the parameter r' (representing the ratio between g' tensor elements), calculated from measurements on the trimer in *A* (blue) and *D* (orange). (*H*) Wavelength dependence of the parameter Δ' (representing the phase difference between g' tensor elements), calculated from measurements on the trimer in *A* (blue) and *D* (orange).

molecule, corresponding to the three junctions formed by pairs of particles. The intensity profile shown in Fig. 2*B* is maximal at an angle of ≈75°, which does not match any of the pairs. Even more unexpectedly, the depolarization ratio profiles (Fig. 2*C*) do not coincide with each other, and in addition they are both rotated with respect to the intensity profile: the polarization pattern of the 555-nm light is rotated by ≈45°, whereas that of the 583-nm light is rotated by ≈75°. We used the GMT to calculate the intensity and depolarization ratio profiles assuming that the molecule is placed in turn in each of the three possible junctions. When the molecule is placed in the junction between particles 2 and 3, marked with an arrow in Fig. 2*A*, the calculation (which, we stress again, uses only the geometry of the aggregate as input) agrees very well with the experimental results. Clearly, particle 1 breaks the axial symmetry of the junction formed by particles 2 and 3, which leads to rotation of the intensity pattern as well as of the polarization of the RS light in a wavelength-dependent manner. Additional observations can now be made: (*i*) The intensity profile never reaches a value close to zero, suggesting that there is enhancement in the junction irrespective of the incident polarization (note that the enhanced local field is, however, always linearly polarized along the dimer axis, see *SI Text* and Fig. S1). (*ii*) The depolarization ratios at both wavelengths never reach ±1, suggesting that the scattered light is elliptically polarized. (*iii*) In contrast to the depolarization ratios, the relative intensity profiles (measured at 555 nm and 583 nm) do not depend on the observation wavelength. This is a confirmation of the fact that the relative intensity of the RS light depends only on the enhancement at the laser frequency (the *g* tensor) if a single molecule contributes to the signal.

A very similar behavior is observed in the case of the trimer shown in Fig. 2*D*. Again both intensity and depolarization ratio profiles are rotated with respect to the axis of the junction containing the molecule (Fig. 2 *E* and *F*, respectively), and the latter also show wavelength dependence. This is again a consequence of a symmetry break in the anisotropic nanocrystal arrangement. Overall ≈10 asymmetric nanocrystal aggregates with complex wavelength-dependent behavior were observed in this work, some of them with more than three particles. Three additional examples are shown in Figs. S3–S5. We have also observed >50 dimers and all of them demonstrated a simple polarization pattern similar to the dimer shown in Fig. 1.

Discussion

We presented strong evidence above that the response of asymmetric silver nanoparticle trimers to electromagnetic radiation, either external or emitted by a molecule residing within the structure, may significantly differ from the simple dipolar response of dimer-like structures. This response leads to rotation of the polarization of light scattered by the trimers, accompanied by a significant deviation from linear polarization. It is important to note that this kind of response depends on the existence of broken symmetry in the geometry of the nanoparticle cluster. Thus, a trimer of equal-sized particles forming an equilateral triangle will present a "standard" dimer-like response. An asymmetric arrangement, like those shown in Fig. 2, guarantees a more complex response. Our experimental observables, namely the intensity and depolarization ratio of RS scattered light, can be rationalized in terms of the two plasmon enhancement tensors, g and g'. Fitting Eqs. **4** and **5** to the experimental patterns we can extract the parameters characterizing the two tensors, namely r, r', Δ and Δ'. These parameters, obtained at a series of wavelengths,[§§] are shown in Fig. 2 *G* and *H* for the two trimers of Fig. 2 *A* and *D*. Note that parameters at $\lambda = 532$ nm (the wavelength of the laser) were extracted from the intensity profiles, whereas those at Stokes-shifted wavelengths were obtained from depolarization ratios. The relation between the g and g' tensors allows us to plot all parameters on the same graph. Interestingly, the parameters of the g' tensor, if measured at the laser frequency, would be the same as the parameters of the g tensor (see Eq. **S1** and Fig. S6). Inversely, parameters of the g tensors at Stokes shifted frequencies can be obtained from corresponding g' tensors. In principle, one can also obtain the enhancement properties at blue-shifted frequencies with respect to the laser line by using anti-Stokes scattering. Thus, Raman scattering can be used as a sensitive meter of the wavelength-dependent plasmon enhancement tensors of nanoparticle clusters, probing a range of frequencies around and including the frequency of the laser used.

What is the meaning of the extracted parameters? First, we note again that irrespective of the values of r and Δ, the enhanced local field is always linearly polarized along the dimer axis (Fig. S1). Second, when $r \ll 1$, $r' \ll 1$, both intensity and depolarization patterns match the dimer case. In general, however, r and Δ need not be zero, which will result in maximal enhancement of the laser field no longer occurring along the symmetry axis of the molecule-containing junction, accompanied by a finite value for the minimal enhancement (as opposed to a value of 0 in the dimer case). For nonzero r' and Δ' the scattered field becomes elliptically polarized and rotated with respect to the junction axis. A particularly interesting extreme case is met when $r = 1$ and simultaneously $\Delta = 90°$, which implies that the intensity profile does not depend on the direction of the incident polarization ($I(\theta) = \text{const.}$), that is, a complete enhancement isotropy is observed. Similarly, when $r' = 1$ and simultaneously $\Delta' = 90°$, the scattered light is circularly polarized and the depolarization ratio is always null [$\rho(\theta) = 0$]. Different degrees of isotropy and elliptical polarization are obtained with other combinations of these parameters.

As seen from Fig. 2 *G* and *H*, the experimentally measured wavelength-dependent parameters r, r′, Δ, and Δ′ are significantly nonzero, which implies that the laser enhancement at the junction is partially isotropic, and that the RS light is elliptically polarized. Interestingly, a systematic variation of these parameters with wavelength is seen—r' increases while Δ' decreases. However, as will be discussed next, the specific form of the wavelength dependence of r' and Δ' depends very much on the geometry of the nanoparticle trimer.

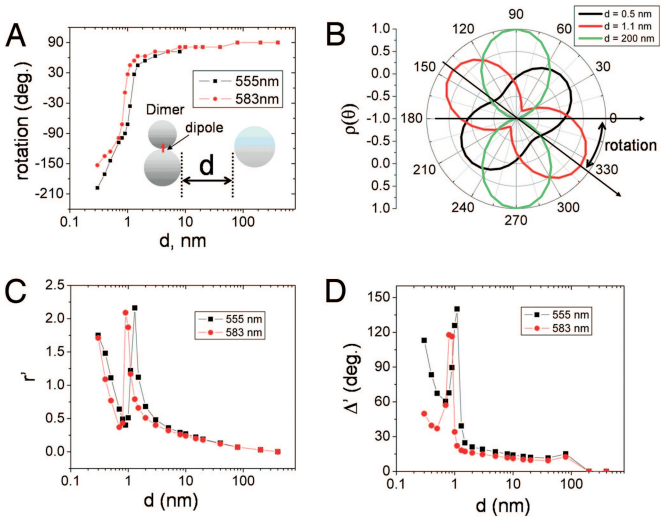

Fig. 3. Polarization rotation as a function of the position of the third particle in a trimer with particle radii of 24 nm, 35 nm, and 40 nm. The distance between the dimer is kept 1 nm to allow the molecule located. (*A*) A calculation showing the polarization rotation as the blue particle in *Inset* approaches the other two particles. When the separation is large ($d > 10$ nm), there is no coupling between the dimer and the blue particle, and hence, the emission is polarized along the dimer axis. When the distance becomes smaller, the polarization is rotated clockwise in a wavelength-dependent fashion. The graph shows the angle of the maximum of the depolarization ratio pattern at two observation wavelengths: $\lambda = 555$ nm (black) and 583 nm (red). Note that ordinate is log-scaled. (*B*) A few of the depolarization ratio patterns at $\lambda = 555$ nm. At $d = 200$ nm (green) the coupling is negligible and the depolarization profile is oriented along the dimer axis. This is, however, not the case at $d = 1.1$ nm and $d = 0.5$ nm (red and black, respectively) where the coupling becomes strong and the depolarization ratio pattern gets rotated clockwise by ≈120° and ≈230°, respectively. (*C*) r' as a function of distance of the blue particle. (*D*) Δ' as a function of the distance of the blue particle.

To further study the role of geometry in determining the level of polarization modulation, we performed a series of GMT calculations in which a molecule was assumed to reside in the junction between two particles, whereas structural properties of the third particle were systematically varied. We first varied the distance of the third particle from the other two. Fig. 3 shows the results of this calculation. When the particle is positioned at a large distance ($d = 200$ nm), the depolarization patterns calculated at two wavelengths coincide with the symmetry axis of the junction between the other two particles (with the maximum at 90°). As the particle is moved closer and closer to the other two, the depolarization patterns are rotated more and more. Three of the depolarization patterns calculated at 555 nm are shown in Fig. 3*B*. Clearly, the degree of ellipticity of the RS light varies with separation between particles. At large d the RS light is linearly polarized (the maximum value of the depolarization ratio is +1), but it becomes significantly elliptically polarized at $d < 1$ nm (the maximum value of the depolarization ratio is <0.5). A similar behavior is observed for scattered light at 583 nm (data not shown). This is also reflected in Fig. 3 *C* and *D* which shows the calculated parameters of the g' tensor. At large separations r' is small and the coupling is weak; therefore, the aggregate behaves essentially as a dimer. At smaller and smaller separations both r' and Δ' gradually increase, finally resulting in a narrow peak at distances around ≈1 nm. This peak implies that polarization modulation is very sensitive to interparticle separation in that region. Note that experimentally observed behav-

[§§]The choice of wavelengths was dictated by the strong Raman peaks of rhodamine 6G, which provide enough intensity for a good signal-to-noise ratio.

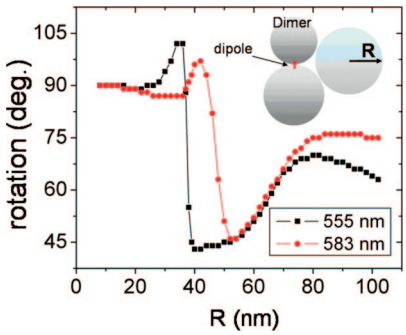

Fig. 4. Polarization rotation as a function of the size of the third particle in a trimer. This calculation shows the effect of changing the radius of the blue sphere in *Inset* in the range between 10 and 100 nm, while keeping all interparticle distances constant at $d = 1$ nm, and the radii for the dimer are 24 nm and 35 nm, respectively. At relatively small sizes ($R < 20$ nm) the depolarization ratio is similar to that obtained from a nanoparticle dimer (this was observed experimentally, see Fig. S7), whereas at larger sizes a nonmonotonic wavelength-dependent polarization rotation occurs.

ior (r' increasing with wavelength, Δ' decreasing with wavelength; see Fig. 2 *G* and *H*) does not hold at every separation, indicating that the exact nanoparticle arrangement plays a crucial role in determining the dependence of the scattered light polarization on wavelength.

We also probed the role of geometry by varying the size of the third particle, now located at a fixed distance from the other two. This calculation was motivated by the observation of the trimer presented in Fig. S7, which showed dimer-like experimental patterns. This behavior was attributed to the fact that the third particle in the arrangement is relatively small, and therefore does not couple strongly enough to modulate the polarization. Fig. 4 presents the results of a calculation in which the size of the third particle was systematically varied. The modulation of the polarization patterns at 555 and 583 nm is indeed a function of this size. This modulation, however, is nonmonotonic with particle size, and it is clear from Fig. 4 that only within a certain range of sizes is the response wavelength-dependent. Note that the size of the additional particle has to be relatively large to observe a significant effect, $R > 30$ nm and $R > 40$ nm for 555-nm and 583-nm scattered light, respectively.

In conclusion, we combined Raman spectroscopy, electron microscopy, and electromagnetic field calculations to show that nanocrystal trimers can interact with light in a complex manner, leading to a wavelength-dependent response. Our observations were facilitated by the ability to measure individual molecules, as well as by the realization that the two plasmon enhancement tensors, namely the laser- and the RS-field enhancement tensors, can be measured separately. Our results indicate that, although the strongest enhancement of EM fields is still obtained in junctions between two particles, symmetry breaking induced by the presence of a third particle may strongly affect the polarization properties of scattered light, because of strong plasmonic coupling between all particles. This coupling depends crucially on the wavelength of the light, the relative sizes of the nanoparticles, and their relative distances. Because the symmetry break is the only condition for anisotropic polarization behavior, similar observations can be expected in any kind of asymmetric clusters (not necessarily trimers). The ability to manipulate the polarization of the Raman light scattered from a single molecule on a nanoscale might be of use in future applications of plasmonics.

Methods

Sample Preparation. Silver colloids were formed by the citrate reduction method of Lee and Meisel (27). The nanocrystals were incubated with 1 nM rhodamine 6G and 1 mM NaCl overnight (in some experiments, an increased concentration of salt, 10 mM, was used to obtain a larger number of aggregates). The aggregates were allowed to absorb from solution for 1 min on polylysine-coated ITO slides meshed by gold grids. These grids, which were prepared on the surface by e-beam lithography, with 10 × 10-μm squares, were used to identify the position of Raman-scattering aggregates in SEM images.

Raman Spectroscopy. A home-built Raman spectrometer was used for polarized SERS measurement. Samples were mounted on an inverted microscope (IX70, Olympus) and excited by using a CW frequency-doubled Nd^{2+}-YVO_4 laser operating at 532 nm (Coherent, Verdi). The linearly polarized laser beam was expanded by means of a long-focal-length lens and directed to the sample through a 100× N.A. = 1.3 oil-immersion objective. Laser intensity at the sample was ≈20 W/cm^2. The same objective collected back-scattered light from the sample. A combination of a dichroic mirror (540dclp, Chroma) and long-pass filter (hq545lp, Chroma) was used to discriminate the Stokes and Rayleigh components of the scattered light. An achromatic $\lambda/2$ waveplate (CVI) was installed right above the dichroic mirror, so that both incident and back-scattered light could be rotated by the same angle. Such a configuration, equivalent to rotation of the sample itself, is not sensitive to polarization-dependent optical elements of the setup (18, 28). A Wollaston prism was used to split the scattered light into parallel and perpendicular components, which were sent into a spectrograph (Acton) and then imaged on a back-illuminated CCD camera (Roper). Images were collected for 5 s at each polarization, so that intensity fluctuations typical of the single-molecule regime were averaged out (although some variations in intensity are still evident in our signals). Thus, a full 360° rotation of polarization took ≈2–3 min. At the low laser intensity used in our experiments molecules typically did not photobleach within this time. Images taken with the spectrograph grating aligned to zeroth order were used to identify the position of hot spots on the grid. Analysis of Raman intensities was carried out after subtraction of a diffuse background that appeared in all spectra (29).

Electron Microscopy. SEM images were collected with a SUPRA 55VP FEG LEO (Zeiss) microscope, equipped with a high-efficiency in-lens detector, typically with electron energy of 5 kV. The ITO substrate enabled us to minimize charging of the sample and obtain images of good resolution. The positions of hot spots found under the light microscope were correlated with SEM images to identify the geometry of particular aggregates.

Calculations. The electromagnetic fields generated by interaction of incident and scattered light with silver aggregates were calculated by using the generalized Mie theory (30). In this extension of Mie's original work (21), the incident and scattered fields are expressed as a sum of vector spherical harmonics, and the self-consistent scattered fields from particles are calculated by the method of order-of-scattering (22, 31). The total local field at any point in the space is the sum of the incident field and coupling fields scattered from all of the nanoparticles in the aggregates. The calculation of the RS field assumed that a molecule, placed in a junction between two particles, scatters a field with dipolar symmetry. This assumption is justified for Raman scattering under molecular resonance conditions. The calculations were performed on sets of spheres arranged in the same manner seen in SEM images. In some cases we modified slightly distances between particles to achieve the best agreement to the experimental data. However, the junction with the molecule in it was kept at 1 nm.

ACKNOWLEDGMENTS. This work was supported by Natural Science Foundation of China Contract 10625418 (to H.X.), Ministry of Science and Technology Contract 2006DFB02020 and 2007CB936800 (to H.X.), the "Bairen" projects of the Chinese Academy of Science (H.X.); in part, by Division of Materials Sciences and Engineering, Office of Basic Energy Sciences, Department of Energy Grant DEFG0205ER46209 (to Z.Z.) and, in part, by National Science Foundation Grant DMR-0606485) (to Z.Z.); in part, by the historic generosity of the Harold Perlman Family (G.H.) and by the Israel Science Foundation. The electron microscopy studies were conducted at the Irving and Cherna Moskowitz Center for Nano and Bio-Nano Imaging at the Weizmann Institute of Science.

1. Ozbay E (2006) Plasmonics: Merging photonics and electronics at nanoscale dimensions. *Science* 311:189–193.
2. Lal S, Link S, Halas NJ (2007) Nano-optics from sensing to waveguiding. *Nat Photon* 1:641.
3. Krenn JR, Weeber JC (2004) Surface plasmon polaritons in metal stripes and wires. *Philos Trans R Soc London Ser A* 362:739–756.
4. Knight MW, *et al.* (2007) Nanoparticle-mediated coupling of light into a nanowire. *Nano Lett* 7:2346–2350.

5. Ebbesen TW, *et al.* (1998) Extraordinary optical transmission through sub-wavelength hole arrays. *Nature* 391:667–669.
6. Lezec HJ, *et al.* (2002) Beaming light from a subwavelength aperture. *Science* 297:820–822.
7. Alaverdyan Y, *et al.* (2007) Optical antennas based on coupled nanoholes in thin metal films. *Nat Phys* 3:884–889.
8. de Abajo FJG (2007) Colloquium: Light scattering by particle and hole arrays. *Rev Mod Phys* 79:1267–1290.
9. Xu HX (2004) Electromagnetic energy flow near nanoparticles. I: Single spheres. *J Quant Spectrosc Radiat Transfer* 87:53–67.
10. Xu HX, Aizpurua J, Käll M, Apell P (2000) Electromagnetic contributions to single-molecule sensitivity in surface-enhanced Raman scattering. *Phys Rev E* 62:4318–4324.
11. Xu HX, Bjerneld EJ, Käll M, Borjesson L (1999) Spectroscopy of single hemoglobin molecules by surface enhanced Raman scattering. *Phys Rev Lett* 83:4357–4360.
12. Nordlander P, *et al.* (2004) Plasmon hybridizaton in nanoparticle dimers. *Nano Lett* 4:899–903.
13. Lassiter JB, *et al.* (2008) Close encounters between two nanoshells. *Nano Lett* 8:1212–1218.
14. Andrew P, Barnes WL (2004) Energy transfer across a metal film mediated by surface plasmon polaritons. *Science* 306:1002–1005.
15. Ringler M, *et al.* (2008) Shaping emission spectra of fluorescent molecules with single plasmonic nanoresonators. *Phys Rev Lett* 100:203002.
16. Gordon R, *et al.* (2004) Strong polarization in the optical transmission through elliptical nanohole arrays. *Phys Rev Lett* 92:037401.
17. Xu HX, Käll M (2003) Polarization-dependent surface-enhanced raman spectroscopy of isolated silver nanoaggregate. *ChemPhysChem* 4:1001–1005.
18. Bosnick KA, Jiang J, Brus LE (2002) Fluctuations and local symmetry in single-molecule rhodamine 6G Raman scattering on silver nanocrystal aggregates. *J Phys Chem B* 106:8096–8099.
19. Sung J, *et al.* (2007) Nanoparticle spectroscopy: Birefringence in two-dimensional arrays of L-shaped silver nanoparticles. *J Phys Chem C* 112:3252–3260.
20. Taminiau TH, Stefani FD, Segerink FB, Van Hulst NF (2008) Optical antennas direct single-molecule emission. *Nat Photonics* 2:234–237.
21. Mie G (1908) Contributions to the optics of turbid media, particularly colloidal metal solutions (Translated from German). *Ann Phys* 25:377–445.
22. Li ZP, Xu HX (2007) Electromagnetic energy flow near metal nanoparticles. II: Algorithms for the calculation of the light scattering of multi-spheres and photon energy transport via linear chains of Ag nanoparticles. *J Quant Spectrosc Radiat Transfer* 103:394–401.
23. Le Ru EC, Meyer M, Etchegoin PG (2006) Proof of single-molecule sensitivity in surface enhanced Raman scattering (SERS) by means of a two-analyte technique. *J Phys Chem B* 110:1944–1948.
24. Etchegoin PG, Galloway C, Le Ru EC (2006) Polarization-dependent effects in surface-enhanced Raman scattering (SERS). *Phys Chem Chem Phys* 8:2624–2628.
25. Michaels AM, Jiang J, Brus L (2000) Ag nanocrystal junctions as the site for surface-enhanced Raman scattering of single Rhodamine 6G molecules. *J Phys Chem B* 104:11965–11971.
26. Shegai TO, Haran G (2006) Probing the Raman scattering tensors of individual molecules. *J Phys Chem B* 110:2459–2461.
27. Lee PC, Meisel D (1982) Adsorption and surface enhanced Raman of dyes on silver and gold sols. *J Phys Chem* 86:3391–3395.
28. Duesberg GS, *et al.* (2000) Polarized Raman spectroscopy on isolated single-wall carbon nanotubes. *Phys Rev Lett* 85:5436–5439.
29. Weiss A, Haran G (2001) Time-dependent single-molecule Raman scattering as a probe of surface dynamics. *J Phys Chem B* 105:12348–12354.
30. Xu HX (2004) Calculation of the near field of aggregates of arbitrary spheres. *J Opt Soc Am A* 21:804–809.
31. Xu HX (2003) A new method by extending Mie theory to calculate local field in outside/inside of aggregates of arbitrary spheres. *Phys Lett A* 312:411.